Nanoscale

RSC Publishing

PAPER

View Article Online
View Journal | View Issue

Artificial leaf structures as a UV detector formed by the self-assembly of ZnO nanoparticles†

Cite this: *Nanoscale*, 2013, **5**, 2864

Fei Wang,[ab] Dongxu Zhao,*[a] Zhen Guo,[ab] Lei Liu,[a] Zhenzhong Zhang[a] and Dezhen Shen[a]

Artificial leaf structures have been fabricated by the self-assembly of ZnO nanoparticles. A hydrothermal method was used to synthesize the nanoparticles. The self-assembly patterns showed asymmetric dendritic morphologies, larger surface-to-volume ratios, a broad absorption band and high resistance. A non-equilibrium two-stage-formation process included diffusion limited aggregation, and the phase-field model was introduced to explain the formation mechanism of the pattern. A high-performance ultraviolet detector was fabricated on the artificial leaf structures, which showed that the current under the irradiation of a UV lamp (1.21 mW cm^{-2}) was about 10^4 times greater than in the dark. The various and functional properties of the pattern show us the vast prospects of potential applications for light harvesting systems and other optical-electric devices.

Received 21st November 2012
Accepted 1st February 2013

DOI: 10.1039/c3nr33748k

www.rsc.org/nanoscale

1 Introduction

Biological structures provide special templates for the development of materials with promising optical, electronic and magnetic properties. In the natural world, green leaves exhibit extremely high light-harvesting. The unique structure of green leaves allows them to absorb the sun-light and promote photosynthesis with high efficiency. Artificial leaf structures have already been applied to solar cells and superhydrophobic surfaces.[1–3] Considering the light absorption of the leaf structures, we designed artificial leaf structures to act as photodetectors with high sensitivity.

As a wide band-gap semiconductor, ZnO is a multifunctional material, which has potential applications in ultraviolet (UV) light emitting diodes,[4] laser diodes,[5] UV detectors,[6,7] gas sensors,[8] *etc.* Because ZnO has extremely high resistance to high-energy particle irradiation, UV photodetectors based on ZnO thin films and nanowires have drawn great attention in recent years. Different device structures, such as metal–semiconductor–metal (MSM),[9] p–n junctions,[10] Schottky diodes[11] and cloth structures[12,13] have been fabricated. In this work, artificial leaf structures have been fabricated by the self-assembly of ZnO nanoparticles. This structure showed high sensitivity for UV light.

2 Experimental section

Self-assembly is the spontaneous process of organizing isolated components into ordered patterns. In this work artificial leaf structures were self-assembled from ZnO nanoparticles synthesized by a hydrothermal method. In this process, zinc acetate [$Zn(CH_3COO)_2 \cdot 2H_2O$] and hexamethylenetetramine ($C_6H_{12}N_4$, HMT) were dissolved in deionized water (18.23 MΩ cm) to form a solution with the concentration of 0.01 M for both materials. Then, the above mixed solution was transferred to a Teflon-lined stainless autoclave. The autoclave was placed into an electric oven maintained at 90 °C, and the reaction times were 8, 16 and 24 hours. After the reaction, the autoclave was taken out of the oven and cooled to room temperature naturally. Finally, the solution in the autoclave was dropped on the Si (or glass) substrates and dried at 60 °C for 30 minutes. To make the UV photodetector, 50 nm thick Au electrodes were deposited onto a glass substrate by vacuum evaporation, and optical lithography was applied to define the interdigitated (IDT) contact pattern.

The morphology of the sample was characterized by field emission scanning electron microscopy (FESEM) equipped with energy-dispersive X-ray spectroscopy (EDX). A transmission electron microscope (TEM), the high resolution TEM images and the selected area electron diffraction (SAED) patterns were obtained on a JEOL JEM-2100F. The photoluminescence (PL) measurement was carried out with a JY-630 micro-Raman spectrometer using the 325 nm line of a He–Cd laser as the excitation source. The typical *I–V* curves were measured by a Keithley 2611A measurement system and a Lakeshore 7707 Hall measurement system for more precise measurements. Time-resolved photocurrent rise and decay was obtained by sudden application and removal of light illumination at the applied bias of 50 V.

[a]*State key laboratory of luminescence and applications, Changchun Institute of Optics, Fine Mechanics and Physics, Chinese Academy of Sciences, 3888 Dongnanhu Road, Changchun 130033, People's Republic of China. E-mail: dxzhao2000@yahoo.com.cn; Fax: +86-431-4627031; Tel: +86-431-86176322*

[b]*Graduate School of the Chinese Academy of Sciences, Beijing 100049, People's Republic of China*

† Electronic supplementary information (ESI) available. See DOI: 10.1039/c3nr33748k

3 Results and discussion

Fig. 1a–c show the FESEM images of the self-assembled samples of ZnO nanoparticles with different growth times of 8, 16 and 24 hours (denoted as samples a, b and c). The insets of Fig. 1a–c are the natural leaves, which are a parallel-veined leaf, feather-veined leaf, and palmate-veined leaf, respectively. All of the FESEM images present leaf-like patterns with regular geometries. In Fig. 1b and c the stems and branches of the leaf veins could be observed clearly. Along the main stems the side branches are almost parallel to each other. The sizes of the branches of sample c are much bigger than those of samples a and b. Fig. 1d–f shows the high resolution SEM images of the side branches. From the images we can clearly see the boundary and inner structures of the patterns, which are composed of nanoparticles.

Fig. 2a and b are the TEM, SAED and HRTEM images of sample b, which show the leaf-like patterns are polycrystalline structures consisting of nanoparticles with diameters of around 5 nm. In Fig. 2b the lattice spacing between adjacent lattice planes is 0.26 nm corresponding to the [0001] direction of ZnO. Fig. 2c is an EDX analysis of the sample. Except the tiny amount of remaining organic elements, only zinc and oxygen could be detected from the sample. This result confirms the sample is ZnO. Fig. 2d shows the optical absorption spectra of the leaf-like pattern self-assembled on a glass substrate and a ZnO thin film deposited onto a glass substrate by a radio-frequency magnetron sputtering technique with the deposition time of an hour for reference. The thickness of the ZnO thin film is about 400 nm, which is roughly equal to the average thickness of the leaf-like pattern with a growth time of 16 hours. A sharp absorption edge located at 375.7 nm appears for both samples, but an obvious difference could be clearly seen in the figure. Besides the strong absorption in the UV region, the ZnO thin film is almost transparent in the visible region. However, for the leaf-like structure a broad absorption band covering the UV and visible light regions could be observed, which is due to the strong scattering of light by ZnO nanoparticles. The broad absorption band implies this structure has potential applications in light-harvesting systems.[14,15]

After sample b was annealed at 800 °C for 1 hour under Ar gas, the morphologies of the sample are almost the same as shown in Fig. 3a and 1b. From the high resolution SEM image (Fig. 3b), ZnO nanoparticles grew bigger after annealing. Fig. S1† shows the XRD patterns of the sample. Before annealing, a broad (002) diffraction peak of ZnO can be observed on the curve. From the Scherrer formula,[16] we know that the average diameter of ZnO nanoparticles before annealing was 8.4 nm, but after annealing, the (002) peak of the sample was enhanced and the average diameter of nanoparticles was 17.4 nm, which agrees with the SEM images that after annealing, the particle size of the sample became bigger. Fig. S2† and Fig. 3c are the TEM and HRTEM images of the annealed sample. We could see the ZnO nanoparticles of the artificial leaf structure combined together and self-assembled and recrystallized toward a single crystal. The annealing causes the recrystallization of ZnO nanoparticles, but does not destroy the leaf-like structures. Fig. 3d shows the PL spectra of the as-grown and annealed samples. For the as-grown samples (red curve), a near-band-edge UV emission peak located at about 370 nm and a broad green peak referring to a deep-level or trap-state emission at about 530 nm were detected. After annealing [Fig. 3d (black)], the visible emission was completely suppressed and only a single near-band-edge UV peak is observed in the spectrum, which means after the recrystallization, the crystal quality of the leaf-like structure was improved. The results revealed the

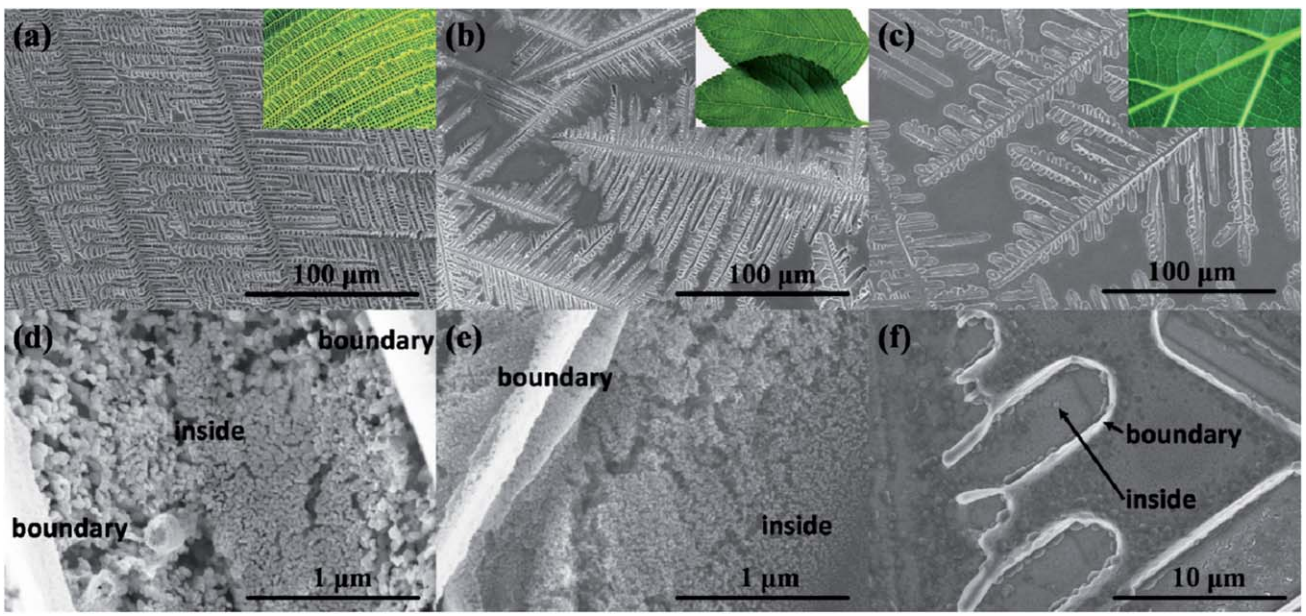

Fig. 1 SEM images of the patterns with the reaction times of 8 h (a), 16 h (b) and 24 h (c). Insets of (a–c) are the pictures of natural leaves. (d–f) The high resolution SEM images of (a–c).

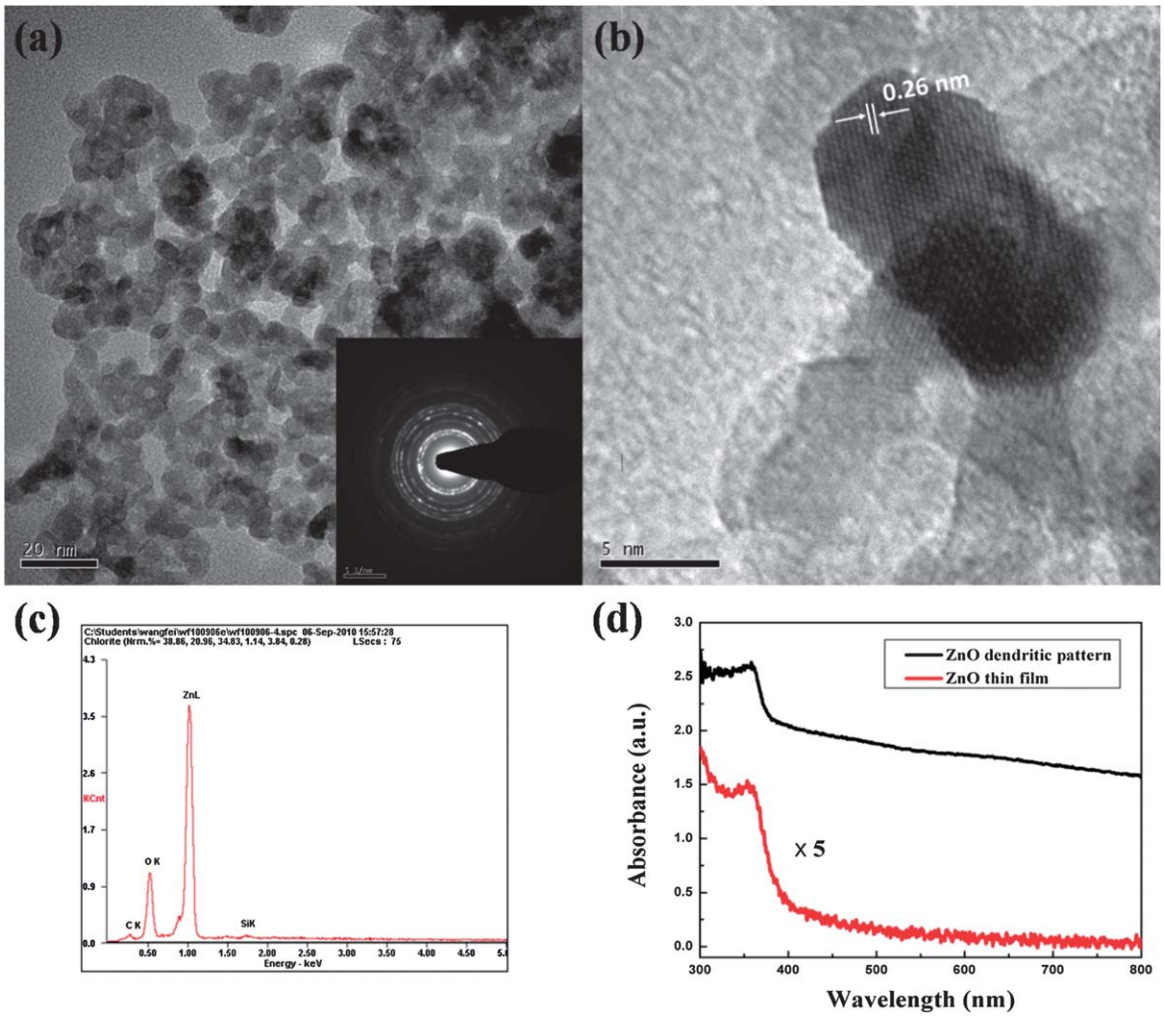

Fig. 2 A TEM image (a) and a HRTEM (b) image of the structure, the inset of (a) is a SAED pattern. (c) An EDX pattern of the sample. (d) The room temperature optical absorbance spectrum of the pattern and referencing thin film, the curve of the ZnO thin film is multiplied by 5.

presence of abundant grain boundaries and defects among nanoparticles, which will strongly affect the performance of its UV detector application.

In order to reveal the formation mechanism of self-assembled dendritic patterns, we should first know the reactions in the solution. In our experiment, hydroxide anions were provided by the hydration of HMT, and the reactions involved in the formation of ZnO were believed to be as follows:

$$(CH_2)_6N_4 + 6H_2O \rightarrow 4NH_3 + 6HCHO \quad (1)$$

$$NH_3 + H_2O \rightarrow NH_4^+ + OH^- \quad (2)$$

$$Zn^{2+} + 2OH^- \rightarrow ZnO + H_2O \quad (3)$$

ZnO growth units were formed following the above equations in the initial growth stage.[17] If a substrate with a ZnO seeds layer was put in the solution, ZnO nanowires could grow on the substrate, which is the typical hydrothermal growth process to obtain nanowires. After this process some nanoparticles would still remain in the solution. After the solution was dropped onto the substrate, the formation of the dendritic patterns began (Fig. 4a).

It is believed that the self-assembly of nanoparticles into leaf-like polycrystalline structures belongs to a non-equilibrium growth process. In this process, diffusion kinetics influence the self-assembly structures on many length scales and determine the macroscopic approach towards the final patterns. The surface tension, surface kinetics and anisotropy occurring at the interface determine the microscopic dynamics on microscopic length scales. The final interfacial shape results from the cooperation of both the microscopic and macroscopic levels.[18] When the solution is dropped on the substrate surface, the solvent begins to evaporate from the substrate. In the initial stage of the drying process, the concentration of the nanoparticles in the solution is low, and the contact line of the drop will be pinned on the hydrophilic substrate.[19] Then, the evaporation proceeds to a certain stage, the contact line is no longer pinned under the ongoing evaporation and will begin to move (Fig. 4b). For the evaporation rate to be larger at the edge, there

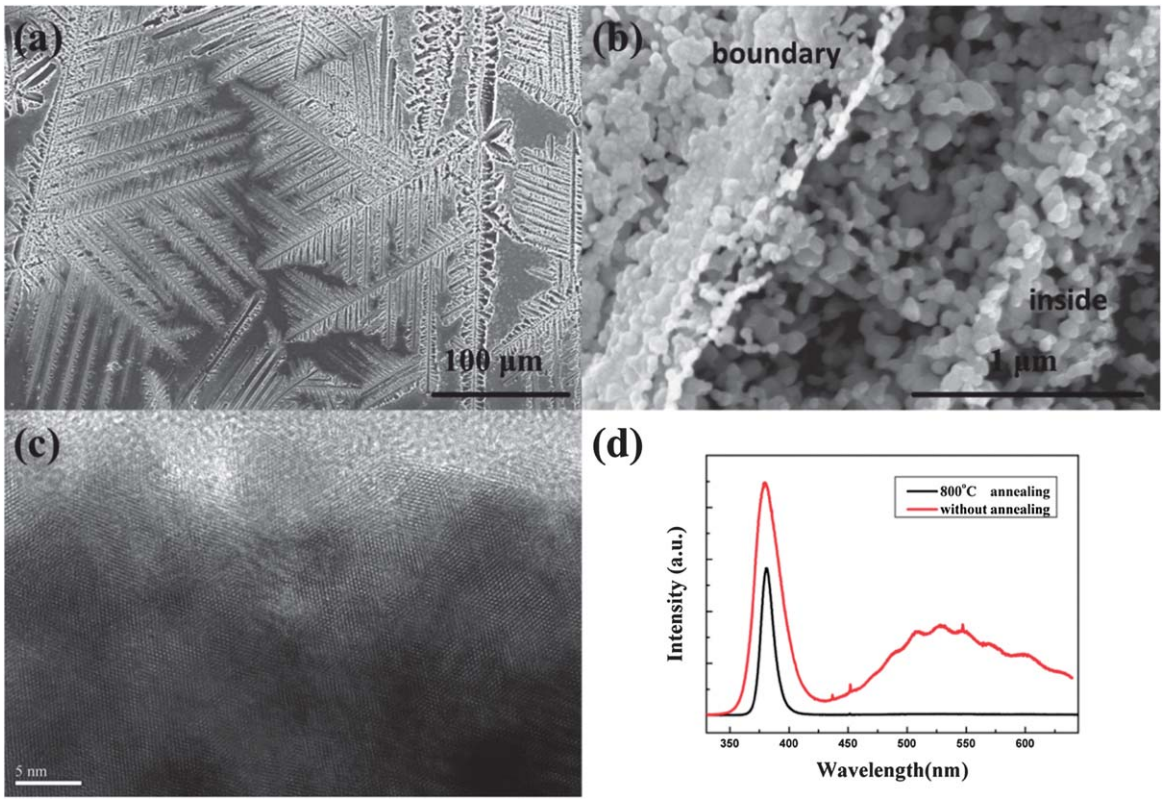

Fig. 3 A SEM image (a) and high resolution SEM image (b) of the crystal structure after annealing. (c) A HRTEM image of the annealed structure. (d) The room temperature PL spectra of the sample.

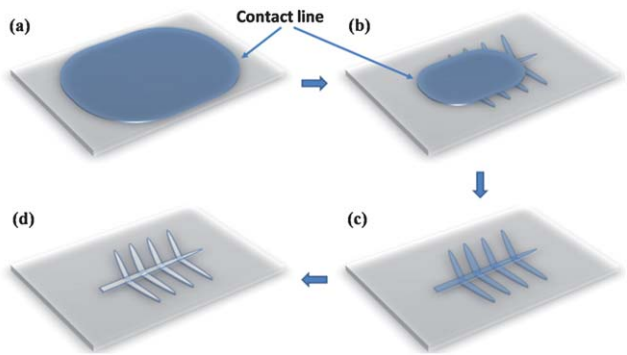

Fig. 4 A schematic description of the formation steps. (a) The solution of nanoparticles is dropped onto the substrate surface. (b) The contact line began to move, the solution at the edge is supersaturated and ZnO nanoparticles together with a small amount of solvent self-assemble into a leaf-like structure. (c) The self-assembled leaf-like structure of nanoparticles together with an amount of solvent. (d) The evaporation of the remaining solvent forms the final dendritic patterns.

must be a flow outward in the drying drop, which replenishes the liquid that is removed from the edge. This flow is capable of transferring 100% of the solute to the contact line and thus accounts for the higher concentration at the edge of the drop. When the solution at the edge is supersaturated, ZnO nanoparticles together with a small amount of solvent will be separated out (Fig. 4c). Similar metal and polymer dendritic structures were fabricated from the undercooling process of melted Ni/Cu and PEO/PMMA blends.[20–23] We can assume that fluids with a certain viscosity, such as the highly concentrated solution, and the melted metal and polymers, have a tendency to form a dendritic structure in their solidification processes.

The formation of our ZnO leaf-like pattern mainly has two stages: firstly, the self-assembly of a viscous fluid, which consists of ZnO nanoparticles and an amount of solvent, into dendritic structures (Fig. 4a–c). Secondly, the evaporation of the remaining solvent to form the final dendritic patterns (Fig. 4d). In the first stage, on a macroscopic scale, the mobility of the nanoparticles in solution is determined by the evaporation rate (ν_{ev}), the translational diffusion rate (ν_t) and the orientational diffusion rate (ν_{or}).[24] The translational diffusion rate controls the number of building blocks moving to the assembly front and forming new grains, the orientational diffusion rate controls the blocks alignment along the crystallographic axes of the grains, and the evaporation rate is related to the freezing rate because nanoparticles will hardly move on a dry surface. In our experiment, we did not introduce any extra electrostatic fields or other force fields, so the diffusion rate at the edge of the drop was isotropic, $\nu_t \approx \nu_{or}$, the nanoparticle diffusion coefficients in solution were also the same, $D_t \approx D_{or}$. When the substrate was heated in an oven, the ν_{ev} was relatively fast and the relative time-scale of evaporation τ was small. In the simulation of E. Rabani *et al.*,[25] when τ/τ_d was small ($\tau_d = \xi^2/D$ that when referring to nanoparticle motion, ξ is the size of the lattice

cell in the model and D is the nanoparticle diffusion coefficients), domain edges were effectively frozen resulting in highly ramified structures, which were similar to diffusion limited aggregation dendritic structures.[26] On a microscopic scale, for dendritic growth, anisotropy is required in the interfacial dynamics and dendritic growth does not occur when surface tension and surface kinetics are isotropic.[18] Considering surface tension anisotropy ε (ε is the amplitude of the angular (θ) dependent contribution to the surface tension γ, $\gamma = \gamma_0[1 + \varepsilon\cos(k\theta)]$), for the phase-field theory,[23] the free energy F is given by the integral

$$F = \int dr\{\alpha^2 T|\Delta\phi|^2 + f + f_{\mathrm{ori}}\},$$

where α is a constant, T is the temperature, ϕ is the structural order parameter (phase field) and f is the local free energy. The solution in our experiment is a pure viscous fluid without any orientation pinning centers, as discussed above, $D_{\mathrm{t}} \approx D_{\mathrm{or}}$, the orientational–translational mobility ratio χ

$$\chi = D_{\mathrm{or}}/D_{\mathrm{t}}$$

is equal to 1, referring to the simulation results of V. Ferreiro *et al.*,[21,23] and is certain to get a symmetrical dendrite pattern.

In the second formation stage, the dendritic pattern of viscous fluid is formed and evaporation of the solvent is ongoing. The decrease of nanoparticles from the boundary to inside the structure is due to the outward flow in the drying structure. The structure size of sample c is larger than sample a and b by many times, as shown in Fig. 1. This is mainly because after a long reaction time, the growth units in solution had nearly run out and the concentration of nanoparticles may dramatically decrease for the reaction time of 24 hours. Highly concentrated suspensions are highly viscous and do not easily flow[27] and so different viscous solutions result in different sizes of the self-assembled patterns. From all of the SEM images of the patterns, we could see the angles between stems and side branches ranged from 30° to 90°, the side branches on one stem were parallel to each other and ones on different stems were not in contact, but apart with a certain space. More than one dendrite morphology is possible, but the final morphology of the pattern is the dynamically fastest forming one.[18,24] It is believed that side branches occur on growing dendrites as a result of selective amplification of microscopic noise present near the dendrite tip,[18,20] but the mechanism remains poorly understood. Further research is needed to understand the origin of this ubiquitous morphology.

The self-assembled leaf-like pattern of ZnO was applied to UV detectors. C. Soci *et al.*[6] and Jin *et al.*[7] have already fabricated visible-blind UV photodetectors on ZnO nanostructures. In our experiment in order to get an efficient electrical contact of a ZnO artificial leaf structure, an Au interdigital electrode was used. The fingers of the Au contact electrodes were 500 μm long and 5 μm wide with 10 μm spacing. Fig. 5a shows the typical *I–V* characteristics of the ZnO dendritic patterns in the dark and under UV illumination ($\lambda = 370$ nm). The ZnO dendritic pattern is very resistive in dark conditions and the current in the dark is

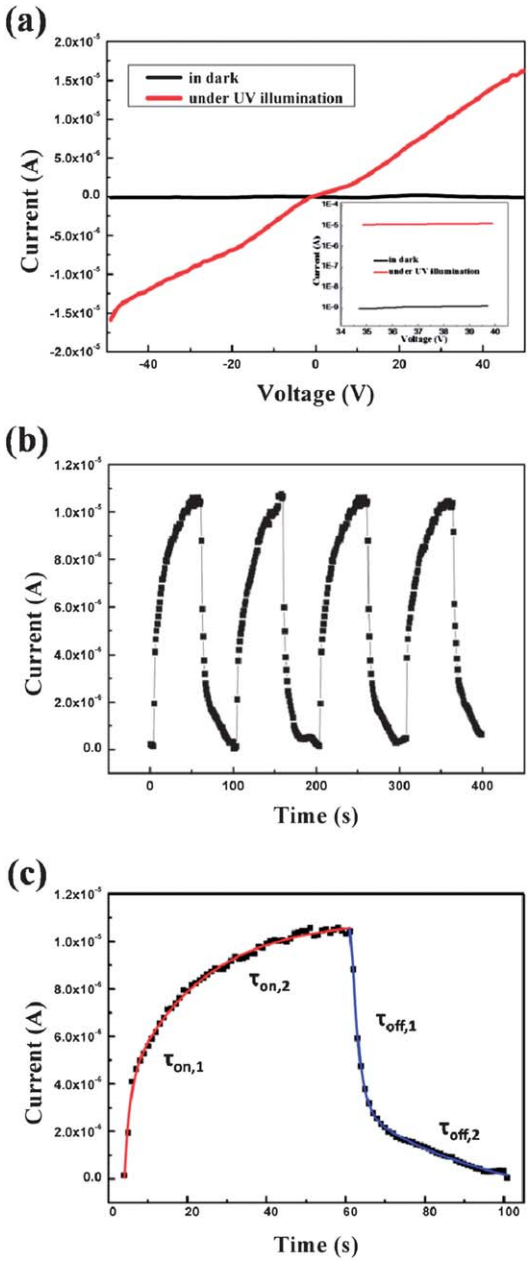

Fig. 5 (a) Typical *I–V* characteristics of the sample, the inset of (a) presents the *I–V* curve on a natural logarithmic scale. (b) Time-resolved photocurrent at the applied bias of 50 V. (c) The biexponential fitting curve of (b).

around 1×10^{-9} A. However, under illumination of a UV light with an average intensity of 1.21 mW cm^{-2}, the current increases significantly to about 1×10^{-5} A. The linear *I–V* curves implies the contact between Au and ZnO is ohmic. The high photocurrent of the device is attributed to the presence of oxygen-related hole-trap states on the surfaces of the nanoparticles, and the light-induced desorption of oxygen from nanoparticle surfaces removes electron traps and increases the free carrier density.[6,7] In the dark, the grain boundaries and the defects, such as dislocations among ZnO nanoparticles result in the high resistance of the dendritic pattern, but when under illumination, the large surface-to-volume ratio of the structure

provides more desorption of oxygen and increases the free carrier density dramatically. Fig. 5b is the time-resolved photocurrent curve of the device in response to turning on and turning off the UV illumination. We used a non-linear fitting program to work out the response time, and the biexponential equation is shown as follows

$$I = I_0 + Ae^{-t/\tau_1} + Be^{-t/\tau_2}$$

where τ_1 and τ_2 are two time constants. The experimental data and the corresponding fitted curves are shown in Fig. 5c, $\tau_{on,1}$ is 1.40 s, $\tau_{on,2}$ is 19.05 s and $\tau_{off,1}$, $\tau_{off,2}$ are 1.81 s and 21.69 s. There are two components of time constants, the faster one is due to the trapping at the surface states and the slower time constant can be attributed to a carrier relaxation process in the deep defect states.[28–30] Due to the large surface-to-volume ratio of the nanoparticles self-assembled structure, the fast time constants of our detector are much lower than the devices in previous works (about 50 s in ref. 28 and 7.0 s in ref. 30). Due to the presence of the grain boundaries and the defects, the slow time constants are higher than the fast constants, but they are also lower than previous works (about 594 s in ref. 28 and 29.7 s in ref. 30).

In summary, we have fabricated dendritic leaf-like structures, which were self-assembled by ZnO nanoparticles. The pattern showed high absorption and low reflectivity due to the strong scattering among nanoparticles and the morphology of the structure. The self-assembly of nanoparticles into dendrite-like polycrystalline patterns were formed according to the non-equilibrium system of diffusion limited aggregation and phase-field models. A UV detector based on the artificial-leaf structure was fabricated, which showed under the irradiation of UV light the photocurrent was about 10^4 times greater than the dark current. The results implied the artificial-leaf structure has potential applications in light harvesting systems and other optical-electric devices.

Acknowledgements

This work is supported by National Basic Research Program of China (973 Program) under Grant nos 2011CB302006, 2011CB302004, the National Natural Science Foundation of China under Grant nos 11074248, 10974197, 10874178, and the 100 Talents Program of the Chinese Academy of Sciences

Notes and references

1 X. Li, T. Fan, H. Zhou, S. K. Chow, W. Zhang, D. Zhang, Q. Guo and H. Ogawa, *Adv. Funct. Mater.*, 2009, **19**, 45.
2 S. Wang, L. Feng and L. Jiang, *Adv. Mater.*, 2006, **18**, 767.
3 Q. Xie, G. Fang, N. Zhao, X. Guo, J. Xu, J. Dong, L. Zhang, Y. Zhang and C. C. Han, *Adv. Mater.*, 2004, **16**, 1830.
4 O. Lupan, P. Pauporte and B. Viana, *Adv. Mater.*, 2010, **22**, 3298.
5 H. Zhu, C. X. Shan, B. Yao, B. H. Li, J. Y. Zhang, Z. Z. Zhang, D. X. Zhao, D. Z. Shen, X. W. Fan, Y. M. Liu and Z. K. Tang, *Adv. Mater.*, 2009, **21**, 1613.
6 C. Soci, A. Zhang, B. Xiang, S. A. Dayeh, D. P. R. Aplin, J. Park, X. Y. Bao, Y. H. Lo and D. Wang, *Nano Lett.*, 2007, **7**, 1003.
7 Y. Jin, J. Wang, B. Sun, J. C. Blakesley and N. C. Greenham, *Nano Lett.*, 2008, **8**, 1649.
8 Q. Wan, Q. H. Li, Y. J. Chen, T. H. Wang and X. L. He, *Appl. Phys. Lett.*, 2004, **84**, 3654.
9 T. K. Lin, S. J. Chang, Y. K. Su, B. R. Huang, M. Fujita and Y. Horikoshi, *J. Cryst. Growth*, 2001, **225**, 110.
10 S. J. Jiao, Z. Z. Zhang, Y. M. Lu, D. Z. Shen and B. Yao, *Appl. Phys. Lett.*, 2006, **88**, 031911.
11 C. S. Lao, J. Liu, P. X. Gao, L. Y. Zhang, D. Davidovic, R. Tummala and Z. L. Wang, *Nano Lett.*, 2006, **6**, 263.
12 B. Liu, Z. Wang, Y. Dong, Y. Zhu, Y. Guo, S. Ran, Z. Liu, J. Xu, Z. Xie, D. Chen and G. Shen, *J. Mater. Chem.*, 2012, **22**, 9379.
13 Z. Wang, H. Wang, B. Liu, W. Qiu, J. Zhang, S. Ran, H. Huang, J. Xu, H. Han, D. Chen and G. Shen, *ACS Nano*, 2011, **5**, 8412.
14 F. Kim, J. H. Song and P. Yang, *J. Am. Chem. Soc.*, 2002, **124**, 14316.
15 H. Sun, H. Wei, H. Zhang, Y. Ning, Y. Tang, F. Zhai and B. Yang, *Langmuir*, 2011, **27**, 1136.
16 A. L. Patterson, *Phys. Rev.*, 1939, **56**, 978.
17 S. Cho, S. H. Jung and K. H. Lee, *J. Phys. Chem. C*, 2008, **112**, 12769.
18 E. B. Jacob and P. Garik, *Nature*, 1990, **343**, 523.
19 R. D. Deegan, O. Bakajin, T. F. Dupont, G. Huber, S. R. Nagel and T. A. Witten, *Phys. Rev. E: Stat. Phys., Plasmas, Fluids, Relat. Interdiscip. Top.*, 2000, **62**, 756.
20 L. M. Williams, M. Muschol, X. Qian, W. Losert and H. Z. Cummins, *Phys. Rev. E: Stat. Phys., Plasmas, Fluids, Relat. Interdiscip. Top.*, 1993, **48**, 489.
21 V. Ferreiro, J. F. Douglas, J. A. Warren and A. Karim, *Phys. Rev. E: Stat., Nonlinear, Soft Matter Phys.*, 2002, **65**, 042802.
22 L. Granasy, T. Pusztal, J. A. Warren, J. F. Douglas, T. Borzsonyl and V. Ferreiro, *Nat. Mater.*, 2003, **2**, 92.
23 L. Granasy, T. Pusztal, T. Borzsonyl, J. A. Warren and J. F. Douglas, *Nat. Mater.*, 2004, **3**, 645.
24 A. Sukhanova, A. V. Baranov, T. S. Perova, J. H. M. Cohen and I. Nabiev, *Angew. Chem., Int. Ed.*, 2006, **45**, 2048.
25 E. Rabani, D. R. Reichman, P. L. Geissler and L. E. Brus, *Nature*, 2003, **426**, 271.
26 T. A. Witten and L. M. Sander, *Phys. Rev. Lett.*, 1981, **47**, 1400.
27 C. Li, M. Akinc, J. Wiench, M. Pruski and C. H. Schilling, *J. Am. Ceram. Soc.*, 2005, **88**, 2762.
28 A. Bera and D. Basak, *Appl. Phys. Lett.*, 2008, **93**, 053102.
29 S. E. Ahn, J. S. Lee, H. Kim, S. Kim, B. H. Kang, K. H. Kim and G. T. Kim, *Appl. Phys. Lett.*, 2004, **84**, 5022.
30 W. Yan, N. Mechau, H. Hahn and R. Krupke, *Nanotechnology*, 2010, **21**, 115501.